Nano Active Stabilization System - Introduction

Dehaeze Thomas

April 17, 2025

Contents

1 Context of this thesis

Synchrotron Radiation Facilities

Accelerating electrons to produce intense X-ray

Synchrotron radiation facilities function as particle accelerator light sources, where electrons are accelerated to near the speed of light. As these electrons traverse magnetic fields, typically generated by insertion devices or bending magnets, they produce exceptionally bright light known as synchrotron light. This intense electromagnetic radiation, particularly in the X-ray spectrum, is subsequently utilized for the detailed study of matter. Approximately 70 synchrotron light sources are operational worldwide, with prominent facilities illustrated in Figure 1.1. The global distribution underscores the significant utility of synchrotron light for the scientific community.

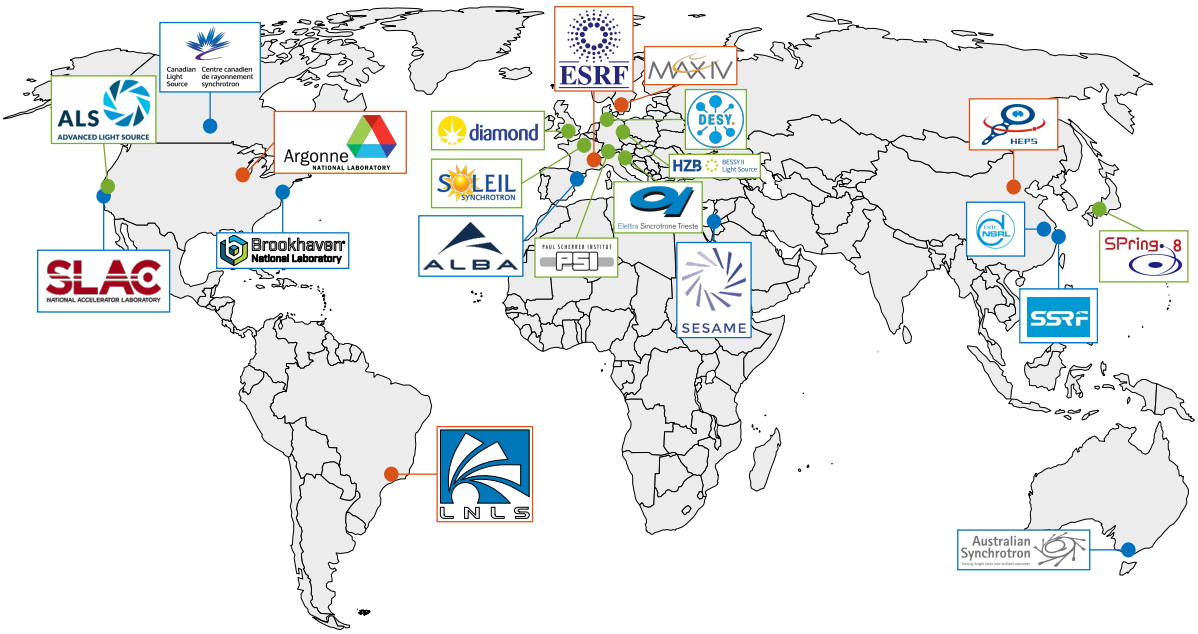

Figure 1.1: Major synchrotron radiation facilities in the world. 3rd generation Synchrotrons are shown in blue. Planned upgrades to 4th generation are shown in green, and 4th generation Synchrotrons in operation are shown in red.

These facilities fundamentally comprise two main parts: the accelerator complex, where electron acceleration and light generation occur, and the beamlines, where the intense X-ray beams are conditioned and directed for experimental use.

The European Synchrotron Radiation Facility

The European Synchrotron Radiation Facility (ESRF), shown in Figure 1.2b, is a joint research institution supported by 19 member countries. Since commencing user operations in 1994, the ESRF was recognized as the world's first third-generation synchrotron source. Its accelerator complex, schematically depicted in Figure 1.2a, includes a linear accelerator, a booster synchrotron for accelerating electrons close to light speed, and an 844-meter circumference storage ring where electrons are maintained for light production. Radiating from the storage ring are over 40 beamlines, each equipped with specialized instrumentation catering to a diverse range of scientific disciplines, including structural biology and materials science under various conditions.

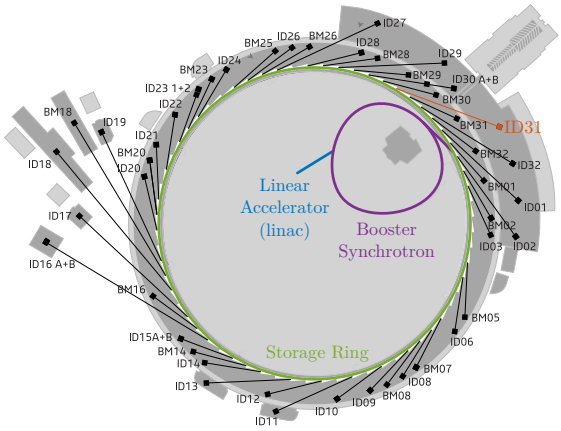

(a) Schematic of the ESRF. The linear accelerator is shown in blue, the booster synchrotron in purple and the storage ring in green. There are over 40 beamlines, the ID31 beamline is highlighted in red

(b) European Synchrotron Radiation Facility

Figure 1.2: Schematic (a) and picture (b) of the European Synchrotron Radiation Facility, situated in Grenoble, France

3rd and 4th Generation Light Sources

In August 2020, following an extensive 20-month upgrade period, the ESRF inaugurated its Extremely Brilliant Source (EBS), establishing it as the world's premier fourth-generation synchrotron [1]. This advancement was predicated on a novel storage ring concept engineered to significantly enhance the brilliance and coherence of the emitted X-ray beams. Brilliance, a key figure of merit for synchrotron sources, experienced an approximate 100-fold increase with the implementation of EBS, as shown in the historical evolution depicted in Figure 1.3. While this enhanced beam quality presents unprecedented scientific opportunities, it concurrently introduces considerable engineering challenges, particularly concerning sample positioning.

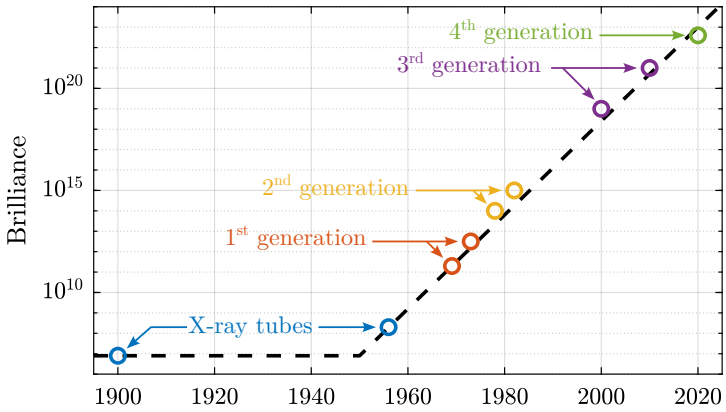

Figure 1.3: Evolution of the peak brilliance (expressed in photons/$s/mm^2/mrad^2/0.1\%BW$) of synchrotron radiation facilities. Note the vertical logarithmic scale.

The ID31 ESRF Beamline

Beamline Layout

The term "beamline layout" encompasses the sequence of optical components situated between the X-ray source (an insertion device in this context) and the sample. Initially, a "white" beam, characterized by high power (often exceeding several kilowatts) and a broad energy spectrum, is generated by the source. This "white" beam is generally unsuitable for direct sample irradiation and is therefore processed through a series of optical elements housed within shielded enclosures known as Optical Hutches (OH), illustrated for ID31 in Figure 1.4. These elements, including absorbers, mirrors, slits, and monochromators, are employed to filter, shape, and select the desired energy range of the X-ray beam. Following the optical hutches, the conditioned beam enters the Experimental Hutch (Figure 1.5a), where, for experiments pertinent to this work, focusing optics are utilized. The sample is mounted on a positioning stage, referred to as the "end-station," which facilitates precise alignment relative to the X-ray beam. Detectors are used to capture the X-rays transmitted through or scattered by the sample. Throughout this thesis, the standard ESRF coordinate system is adopted, wherein the X-axis aligns with the beam direction, Y is transverse horizontal, and Z is vertical upwards against gravity.

Positioning End Station: The Micro-Station

The specific end-station employed on the ID31 beamline is designated the "micro-station". As depicted in Figure 1.5b, it comprises a stack of positioning stages: a translation stage (blue), a tilt stage (red), a spindle for continuous rotation (yellow), and a micro-hexapod (purple). The sample itself (cyan), potentially housed within complex sample environments (e.g., for high pressure or varying temperatures) and weighing up to 50kg, is mounted on top of this assembly. Each stage serves distinct positioning functions; for example, the micro-hexapod enables fine static adjustments, while the Ty translation and Rz rotation stages are utilized for specific scan types. The design objectives prioritized maximum stiffness and minimal positioning errors across its operational stroke. The main components within the experimental hutch—focusing optics, sample stage, sample, and detector—are affixed to a common granite base for enhanced stability, as shown in Figure 1.5a.

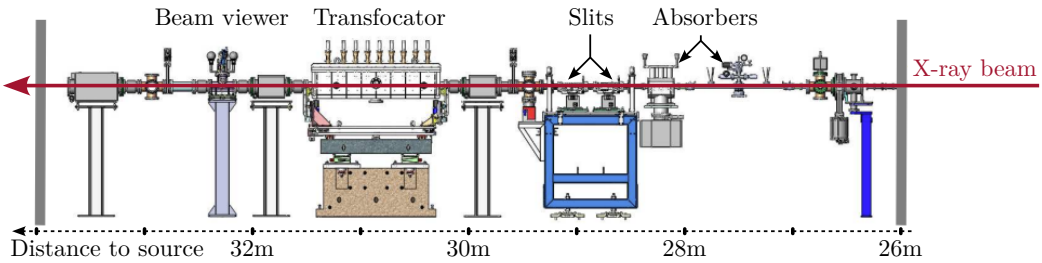

(a) OH1

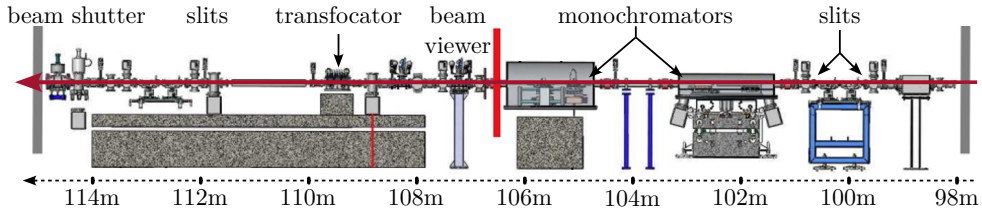

(b) OH2

Figure 1.4: Schematic of the two ID31 optical hutches: OH1 (a) and OH2 (b). Distance from the source (the insertion device) is indicated in meters.

Example of Scientific experiments performed on ID31

The high mobility afforded by the multi-stage configuration of the micro-station enables diverse imaging techniques. Two illustrative examples are provided.

Firstly, tomography experiments are conducted as illustrated schematically in Figure 1.6a. In this technique, the sample is placed in the X-ray beam path, and its orientation is controlled via a rotation stage. Projection images are acquired by the detector at numerous discrete angular positions. Provided the point of interest within the sample remains accurately centered on the beam throughout the rotation, a three-dimensional reconstruction, such as the one presented in Figure 1.6b, can be generated [2].

Secondly, mapping or scanning experiments are performed, often involving focused X-ray beams, as depicted in Figure 1.7a. The sample is translated, typically in the plane perpendicular to the beam (Y and Z directions), while data is collected at each position. An example [3] of a resulting two-dimensional map, acquired with 20nm step increments, is shown in Figure 1.7b. The fidelity and resolution of such images are intrinsically linked to the focused beam size and the precision with which the sample position relative to the beam can be maintained. Positional instabilities, such as vibrations and thermal drifts, inevitably lead to blurring and distortion in the acquired data. Other advanced imaging modalities practiced on ID31 include reflectivity, diffraction tomography, and small/wide-angle X-ray scattering (SAXS/WAXS).

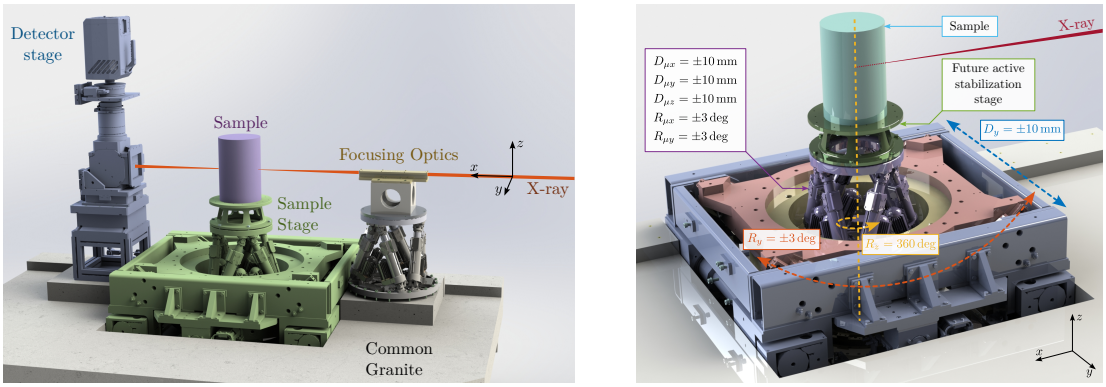

(a) Experimental Hutch **(b)** Micro-Station

Figure 1.5: CAD view of the ID31 Experimal Hutch (a). There are typically four main elements: the focusing optics in yellow, the sample stage in green, the sample itself in purple and the detector in blue. All these elements are fixed to the same granite. CAD view of the The micro-station with the associated degrees of freedom (b).

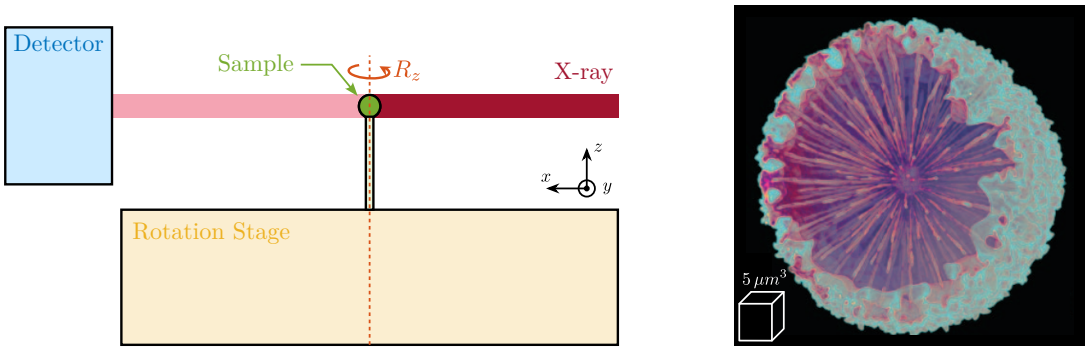

(a) Experimental setup **(b)** Obtained image [2]

Figure 1.6: Exemple of a tomography experiment. The sample is rotated and images are taken at several angles (a). Example of one 3D image obtained after tomography (b).

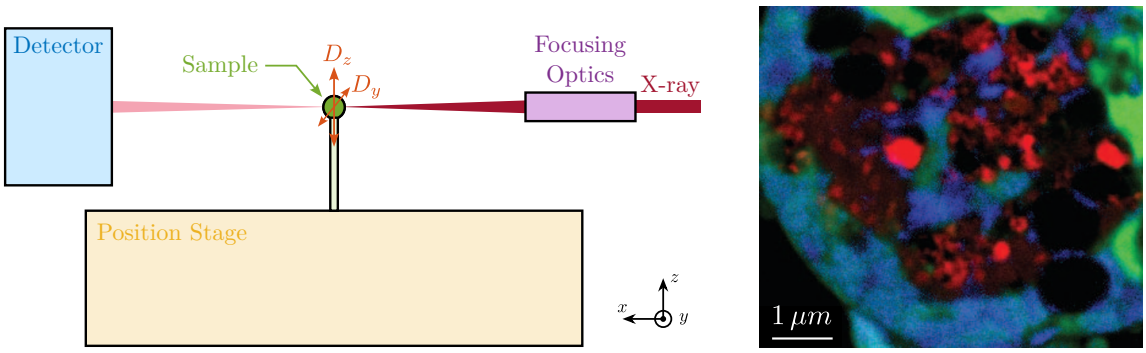

(a) Experimental setup **(b)** Obtained image [3]

Figure 1.7: Exemple of a scanning experiment. The sample is scanned in the Y-Z plane (a). Example of one 2D image obtained after scanning with a step size of 20nm (b).

Need of Accurate Positioning End-Stations with High Dynamics

A push towards brighter and smaller beams

Continuous advancements in both synchrotron source technology and X-ray optics have led to the availability of smaller, more intense, and more stable X-ray beams. The ESRF-EBS upgrade, for instance, resulted in a significantly reduced source size, particularly in the horizontal dimension, coupled with increased brilliance, as illustrated in Figure 1.8.

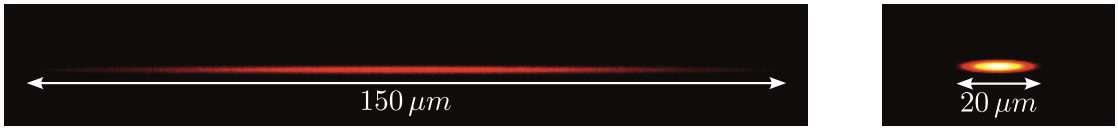

(a) 3^{rd} generation **(b)** 4^{th} generation

Figure 1.8: View of the ESRF X-ray beam before the EBS upgrade (a) and after the EBS upgrade (b). The brilliance is increased, whereas the horizontal size and emittance are reduced.

Concurrently, substantial progress has been made in micro- and nano-focusing optics since the early days of ESRF, where typical spot sizes were on the order of 10 μm [4]. Various technologies, including zone plates, Kirkpatrick-Baez mirrors, and compound refractive lenses, have been developed and refined, each presenting unique advantages and limitations [5]. The historical reduction in achievable spot sizes is represented in Figure 1.9. Presently, focused beam dimensions in the range of 10 to 20 nm (Full Width at Half Maximum, FWHM) are routinely achieved on specialized nano-focusing beamlines.

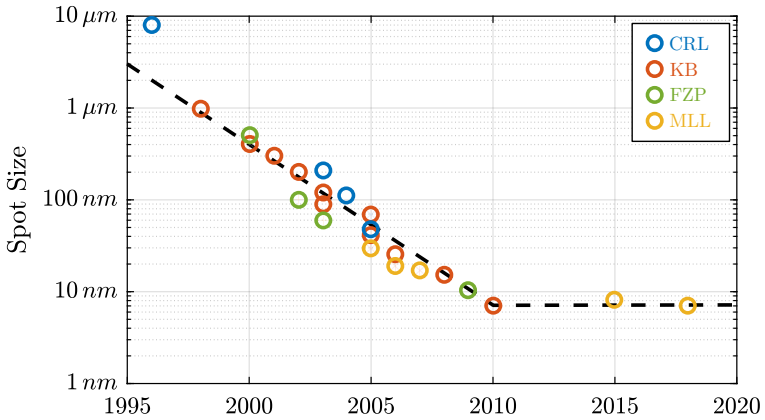

Figure 1.9: Evolution of the measured spot size for different hard x-ray focusing elements. CRL, KB, FZP, MLL. Adapated from [6]

New Dynamical Positioning Needs

The increased brilliance and flux density associated with modern synchrotron sources exacerbate the issue of radiation damage, particularly for sensitive samples and at high-energy beamlines like ID31. Consequently, prolonged exposure of a single sample area to the focused beam must be avoided. Traditionally, experiments were conducted in a "step-scan" mode, illustrated in Figure 1.10a. In this mode, the sample is moved to the desired position, the detector acquisition is initiated, and a beam shutter

is opened for a brief, controlled duration to limit dose before closing; this cycle is repeated for each measurement point. While effective for mitigating radiation damage, this sequential process can be time-consuming, especially for high-resolution maps requiring numerous points.

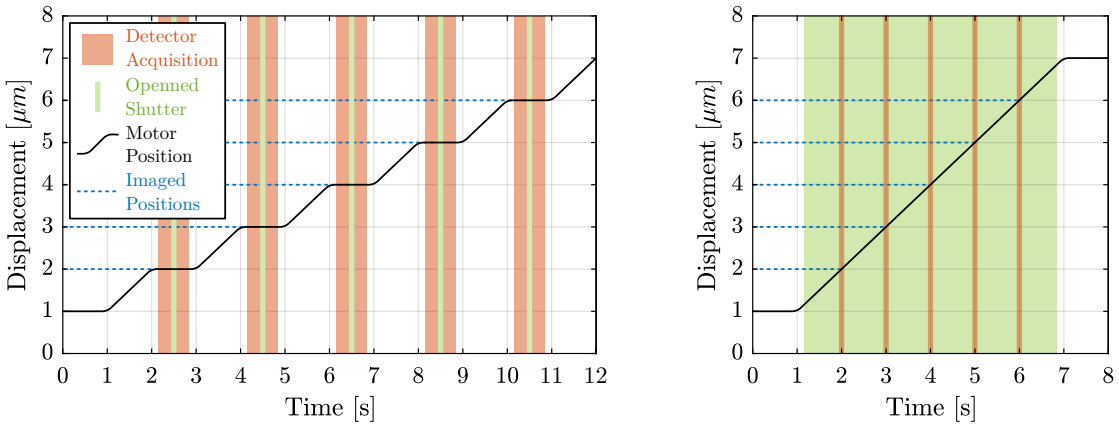

(a) Step by step scan

(b) Fly scan

Figure 1.10: Two acquisition modes. In step-by-step mode (a), the motor moves at the wanted imaged position, the detector acquisition is started, the shutter is openned briefly to have the wanted exposition, the detector acquisition is stopped, and the motor can move to a new position. In *fly-scan* mode (b), the shutter is openned while the sample is in motion, and the detector is acquired only at the wanted positions, on the *fly*.

An alternative, more efficient approach is the "fly-scan" or "continuous-scan" methodology [7], depicted in Figure 1.10b. Here, the sample is moved continuously while the detector is triggered to acquire data "on the fly" at predefined positions or time intervals. This technique significantly accelerates data acquisition, enabling better utilization of valuable beamtime and potentially finer spatial sampling [8].

Furthermore, recent developments in detector technology have yielded sensors with improved spatial resolution, lower noise characteristics, and substantially higher frame rates [9]. Whereas typical integration times for scanning or tomography experiments were previously in the range of 0.1 to 1 second, modern detectors permit integration times on the order of milliseconds, corresponding to frame rates of 100 Hz or higher. This reduction in integration time has two major implications for positioning requirements. Firstly, for a given spatial sampling ("pixel size"), faster integration necessitates proportionally higher scanning velocities. Secondly, the shorter integration times make the measurements more susceptible to high-frequency vibrations. Previously, longer integration effectively averaged out rapid positional fluctuations, resulting in an apparently larger but stable effective X-ray beam. With millisecond-scale integration, however, vibrations up to the kilohertz range can significantly degrade data quality. Therefore, not only must the sample position be stable against long-term drifts, but it must also be actively controlled to minimize vibrations, especially during dynamic fly-scan acquisitions.

Existing Nano Positioning End-Stations

To contextualize the system developed within this thesis, a brief overview of existing strategies and technologies for high-accuracy, high-dynamics end-stations is provided. The aim is to identify the specific characteristics that distinguish the proposed system from current state-of-the-art implementations.

End-Station with Stacked Stages

Positioning systems can be broadly categorized based on their kinematic architecture, typically serial or parallel, as exemplified by the 3-Degree-of-Freedom (DoF) platforms in Figure 1.11. Stacked stages, representing serial kinematics (Figure 1.11a), offer decoupled control for each DoF and generally provide larger ranges of motion. However, positioning errors (e.g., guiding inaccuracies, thermal expansion) accumulate through the stack, compromising overall accuracy. Similarly, the overall dynamic performance (stiffness, resonant frequencies) is limited by the softest component in the stack, often resulting in poor dynamic behavior when many stages are combined.

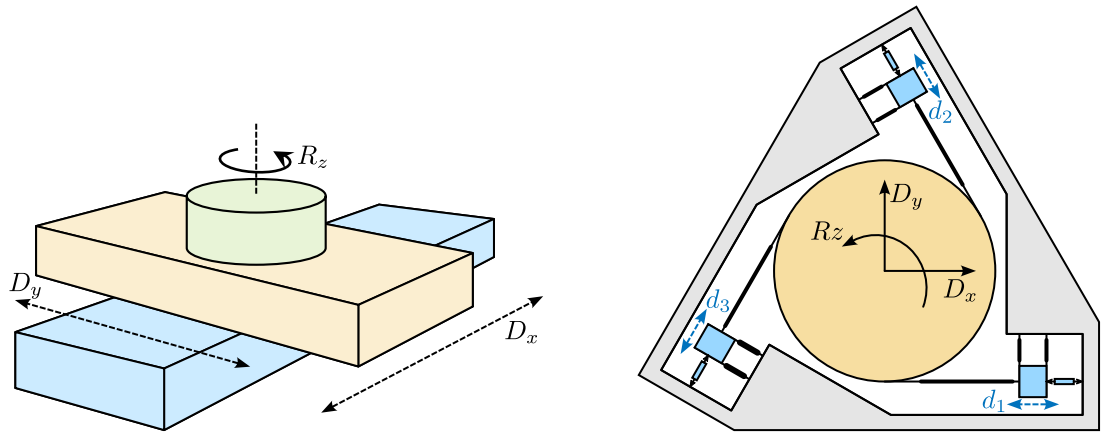

(a) Serial Kinematics **(b)** Parallel Kinematics

Figure 1.11: Two positioning platforms with $D_x/D_y/R_z$ degrees of freedom. One is using serial kinematics (a), while the other uses parallel kinematics (b)

Conversely, parallel kinematic architectures (Figure 1.11b) involve the coordinated motion of multiple actuators to achieve the desired end-effector pose. While theoretically capable of similar DoFs, practical implementations are often restricted to smaller workspaces. The primary advantage lies in significantly higher structural stiffness and consequently superior dynamic performance.

Due to the requirement for extensive mobility in many synchrotron experiments, most end-stations are constructed using stacked stages. Achieving acceptable stability and accuracy in such systems relies heavily on the inherent precision of individual components and environmental control. Strategies include employing a limited number of high-performance stages, such as air-bearing spindles [10], and maintaining extremely stable thermal environments within the experimental hutch, often requiring extended stabilization times [11]. Examples of such end-stations, including those at beamlines ID16B [12] and ID11 [13], are shown in Figure 1.12. However, when a large number of DoFs are required, the cumulative errors and limited dynamic stiffness of stacked configurations can make experiments with nano-focused beams extremely challenging or infeasible.

Online Metrology

The concept of employing external metrology systems to measure and potentially correct for positioning errors is well-established. Ideally, the relative position between the sample's point of interest and the X-ray beam focus would be measured directly. In practice, direct measurement is often impossible;

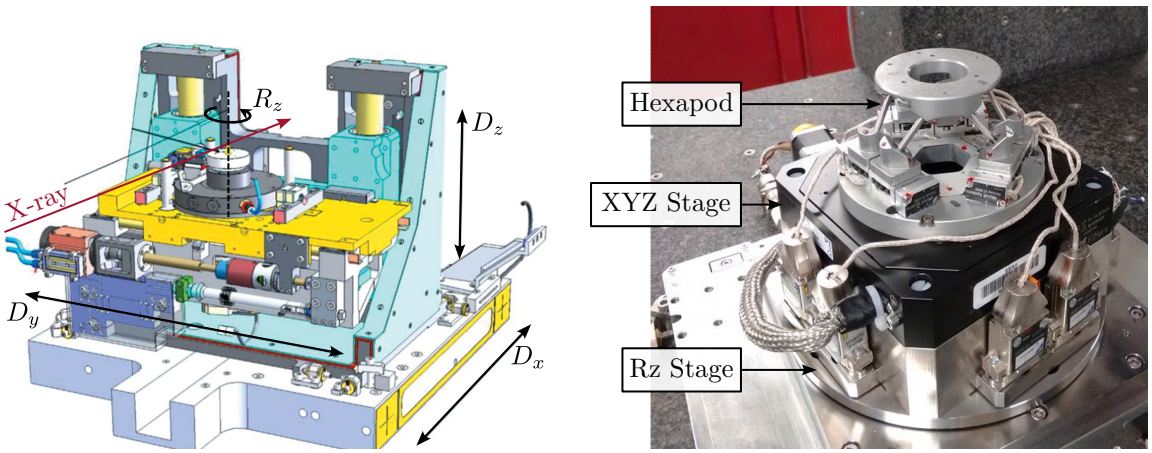

(a) ID16b **(b)** ID11

Figure 1.12: Example of two nano end-stations without online metrology: (a) [12] and (b) [13]

instead, the sample position is typically measured relative to a reference frame associated with the focusing optics or defining apertures, providing an indirect measurement.

This metrology data can be utilized in several ways: for post-processing correction of acquired data; for calibration routines to compensate for repeatable, systematic errors; or, most relevantly here, for real-time feedback control. For applications demanding precise position control, such as maintaining a nanoparticle within a nano-beam during tomography, real-time feedback is essential. Various sensor technologies have been employed, with capacitive sensors [14], [15], [16] and, increasingly, fiber-based interferometers [7], [16], [17], [18], [19], [20], [21], [22], [23], [24] being prominent choices.

Two examples illustrating the integration of online metrology are presented in Figure 1.13. The system at NSLS X8C utilized capacitive sensors for rotation stage calibration and image alignment during tomography post-processing [25]. The PtiNAMi microscope at DESY P06 employs interferometers directed at a spherical target below the sample for position monitoring during tomography, with plans for future feedback loop implementation [16].

Active Control of Positioning Errors

For applications requiring active compensation of measured errors, particularly with nano-beams, feedback control loops are implemented. Actuation is typically achieved using piezoelectric actuators [15], [17], [20], [21], [22], 3-phase linear motors [18], [19], or voice coil actuators [23], [24]. In published studies, feedback bandwidth specifications are often omitted. Historically, the feedback bandwidth reported for such systems has often been relatively low (around 1 Hz), primarily targeting the compensation of slow thermal drifts. More recently, higher bandwidths (up to 100 Hz) have been demonstrated, particularly with the use of voice coil actuators [23], [24].

Figure 1.14 showcases two end-stations incorporating online metrology and active feedback. The ID16A system at ESRF (Figure 1.14a) uses capacitive sensors and a piezoelectric hexapod to compensate for rotation stage errors and perform accurate scans [15]. Another example, shown in Figure 1.14b, employs interferometers and piezoelectric stages to compensate for thermal drifts [17], [26]. A more comprehensive review of actively controlled end-stations is provided in Section [...].

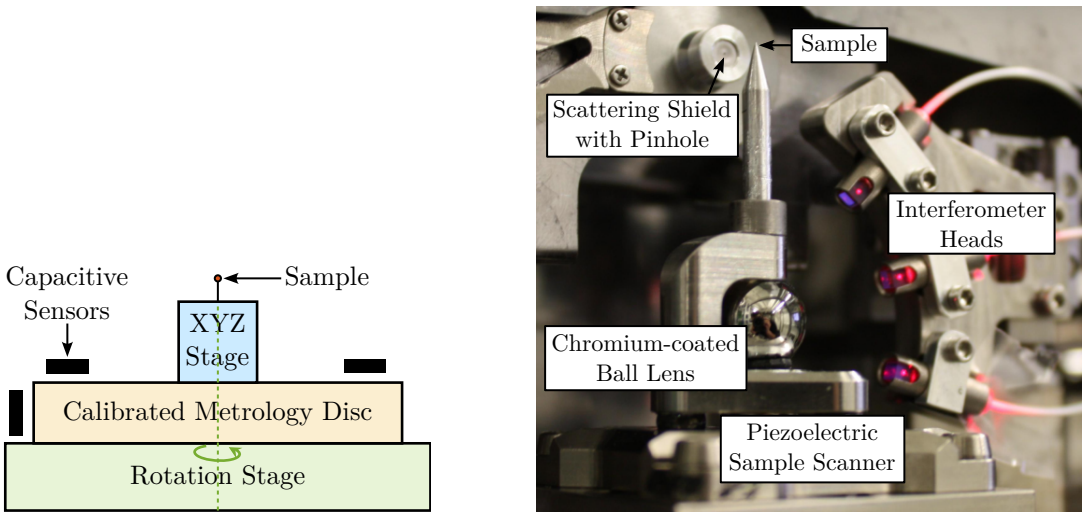

(a) Wang **(b)** Schroer

Figure 1.13: Two examples of end-station with integrated online metrology. (a) [25] and (b) [14]

For tomography experiments, correcting spindle guiding errors is critical. Correction stages are typically placed either below the spindle [7], [15], [18], [19], [20], [21], [22] or above it [14], [16], [24], [25]. In most reported cases, only translational (XYZ) corrections are applied. Payload capacities for these high-precision systems are usually limited, typically handling calibrated samples on the micron scale, although capacities up to 500g have been reported [20], [23]. The system developed in this thesis aims for payload capabilities approximately 100 times heavier (up to 50 kg) than previous stations.

Long Stroke - Short Stroke architecture

End-stations integrating online metrology for active nano-positioning often exhibit limited operational ranges, typically constrained to a few degrees of freedom with strokes around $100\,\mu m$. An alternative strategy involves a "long stroke-short stroke" architecture, illustrated conceptually in Figure 1.15. In this configuration, a high-accuracy, high-bandwidth short-stroke stage is mounted on top of a less precise long-stroke stage. The short-stroke stage actively compensates for errors based on metrology feedback, while the long-stroke stage provides the coarse, large-range motion. This approach allows combining extended travel with high precision and good dynamic response, but is often implemented for only one or a few DoFs, as seen in Figures 1.16a and 1.16b.

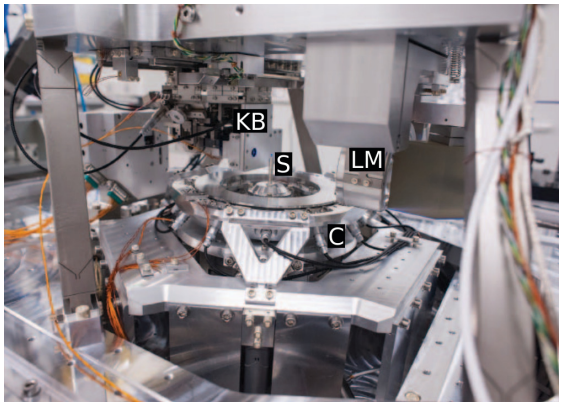

(a) ID16a. =KB= is the focusing optics, =S= the sample, =C= the capacitive sensors and =LM= is the light microscope

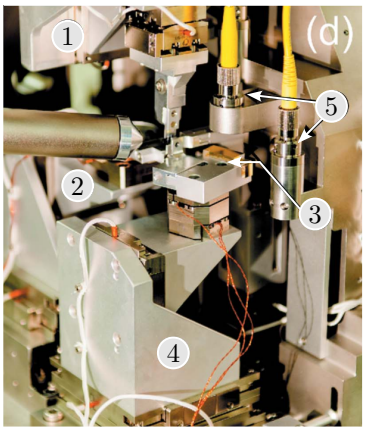

(b) 1 and 2 are stage to position the focusing optics. 3 is the sample location, 4 the sample stage and 5 the interferometers

Figure 1.14: Example of two end-stations with real-time position feedback based on an online metrology. (a) [15]. (b) [17], [26]

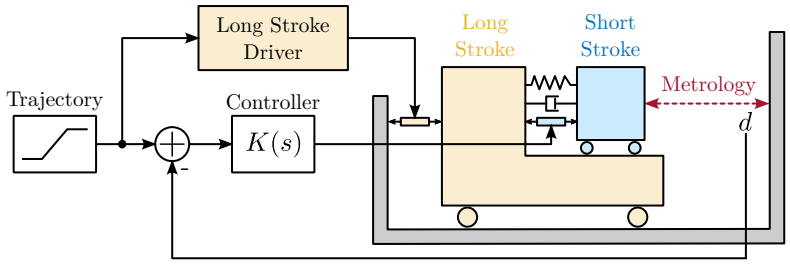

Figure 1.15: Typical Long Stroke - Short Stroke architecture. The long stroke stage is ...

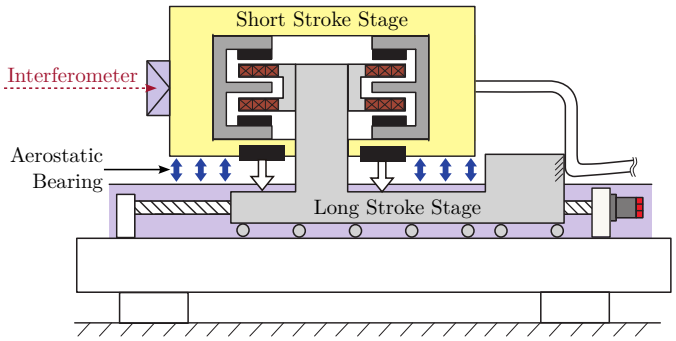

(a) Two stage control with classical stage and voice coil

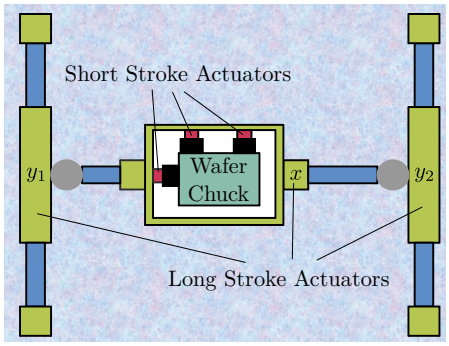

(b) H-bridge. y_1, y_2 and x are 3-phase linear motors. Short stroke actuators are voice coils.

Figure 1.16: (a) [27], (b) [28]

2 Challenge definition

The advent of fourth-generation light sources, coupled with advancements in focusing optics and detector technology, imposes stringent new requirements on sample positioning systems. For the ID31 beamline, the smallest anticipated beam size is approximately 200 nm (horizontal, Dy) by 100 nm (vertical, Dz). To effectively utilize such beams, the positioning system must maintain the sample's point of interest within the beam profile throughout the experiment. This translates to required peak-to-peak positioning stability better than 200 nm in Dy and 100 nm in Dz, corresponding to RMS values of approximately 30 nm and 15 nm, respectively. Furthermore, tilt errors (Ry) must be controlled to below approximately 1.7 µrad peak-to-peak (250 nrad RMS).

Crucially, these specifications must be met even when considering high-frequency vibrations, owing to the use of high-frame-rate detectors. These demanding stability requirements must be achieved within the specific context of the ID31 beamline, which necessitates building upon the existing micro-station infrastructure, accommodating a wide range of experimental configurations requiring high mobility, and handling substantial payloads up to 50 kg.

The existing micro-station, despite being composed of high-quality stages, exhibits positioning accuracy limited to approximately 10 μm and 10 μrad due to inherent factors such as backlash, mechanical play, thermal expansion, imperfect guiding, and vibrations. While individual stage encoders can correct motion along their primary axis, they do not compensate for parasitic motions in other degrees of freedom. The primary objective of this project is therefore defined as enhancing the positioning accuracy and stability of the ID31 micro-station by roughly two orders of magnitude, to fully leverage the capabilities offered by the ESRF-EBS source and modern detectors, without compromising its existing mobility and payload capacity.

The Nano Active Stabilization System Concept

To address these challenges, the concept of a Nano Active Stabilization System (NASS) is proposed. As schematically illustrated in Figure 2.1, the NASS comprises four principal components integrated with the existing micro-station (yellow): a 5-DoF online metrology system (red), a 5- or 6-DoF active stabilization platform (blue), and the associated control system and instrumentation (purple). This system essentially functions as a high-performance, multi-axis vibration isolation and error correction platform situated between the micro-station and the sample. It actively compensates for positioning errors measured by the external metrology system. The overarching goal is to improve the effective positioning accuracy from the micro-station's native $\approx 10\,\mu m$ level down to below 100 nm, while preserving the full mobility and 50 kg payload capability of the underlying stages.

Online Metrology system

The performance of the NASS is fundamentally reliant on the accuracy and bandwidth of its online metrology system, as the active control is based directly on these measurements. This metrology

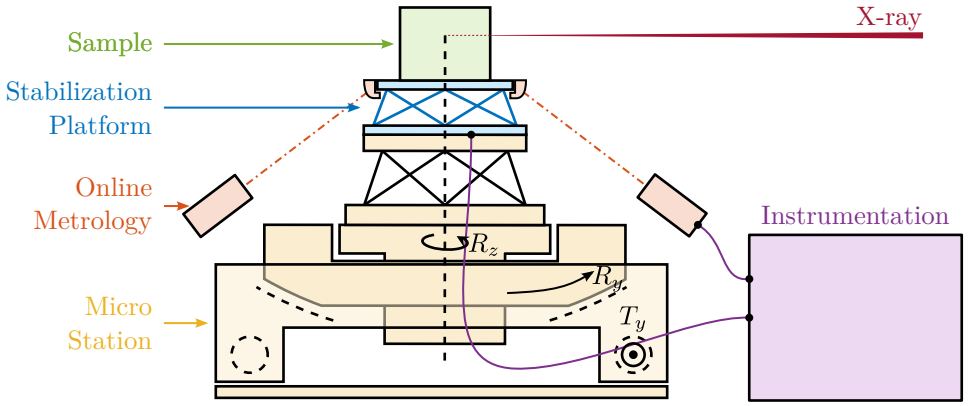

Figure 2.1: The Nano Active Stabilization System concept

system must fulfill several criteria: measure the sample position in 5 DoF (excluding rotation about the vertical Z-axis); ideally, measure position relative to the X-ray focusing optics; possess a measurement range compatible with the micro-station's extensive mobility and continuous spindle rotation; achieve accuracy commensurate with the sub-100 nm positioning target; and offer high bandwidth for real-time control.

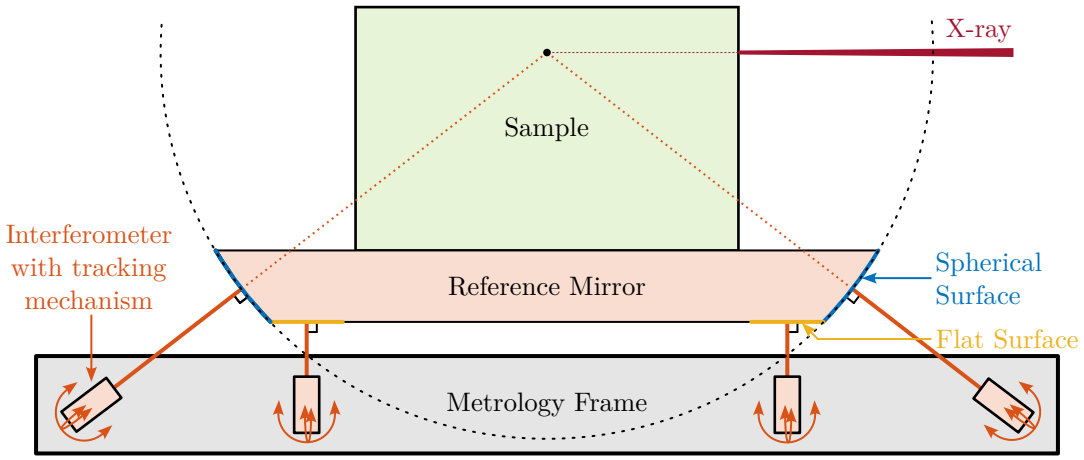

Figure 2.2: 2D representation of the NASS metrology system.

An initial concept, depicted in Figure 2.2, involves a spherical reflector with a flat bottom surface fixed beneath the sample. The sphere's center is intended to coincide with the X-ray focus. Fiber interferometers are directed at both the spherical and flat surfaces. A tracking system is needed to maintain interferometer alignment, eliminating Abbe errors by measuring directly relative to the point of interest. Translational positions (XYZ) are derived from measurements on the spherical surface, while tilt angles (Rx/Ry) are determined from measurements on the flat bottom surface. The development of this complex metrology system constitutes a significant mechatronic project in itself and is currently ongoing; it is not further detailed within this thesis. For the work presented herein, the metrology system is assumed to provide accurate, high-bandwidth 5-DoF position measurements.

Active Stabilization Platform

The active stabilization platform, positioned between the micro-station top plate and the sample, must satisfy several demanding requirements. It needs to provide active motion compensation in 5 DoF (Dx, Dy, Dz, Rx, Ry). It must possess excellent dynamic properties to enable high-bandwidth control capable of suppressing vibrations and tracking desired trajectories with nanometer-level precision. Consequently, it must be free from backlash and play, and its active components (e.g., actuators) should introduce minimal vibrations. Critically, it must reliably support and actuate payloads up to 50 kg.

A suitable candidate architecture for this platform is the Stewart platform (or hexapod), a parallel kinematic mechanism capable of 6-DoF motion. Stewart platforms are widely employed in positioning and vibration isolation applications due to their inherent stiffness and potential for high precision. Various designs exist, differing in geometry, actuation technology, sensing methods, and control strategies, as exemplified in Figure 2.3. A central challenge addressed in this thesis is the optimal mechatronic design of such an active platform tailored to the specific requirements of the NASS.

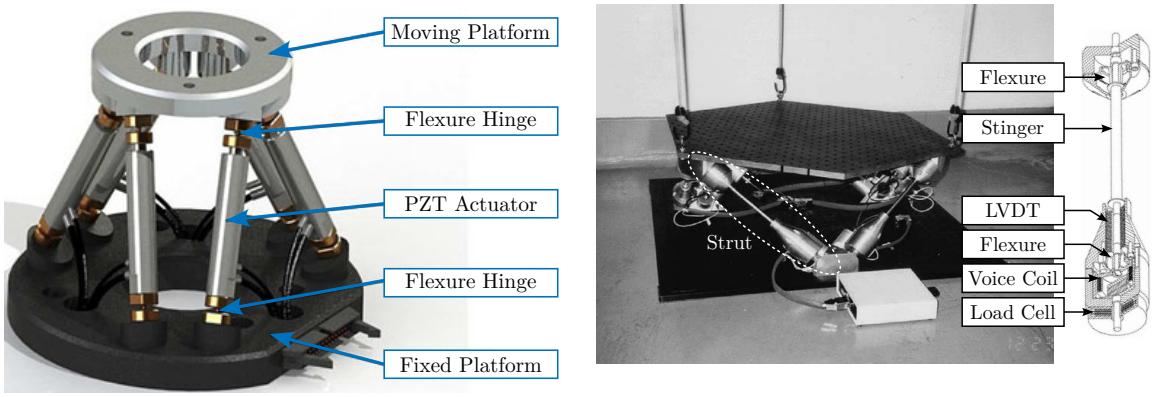

(a) PZT based, for positioning purposes

(b) Voice coil based, Cubic architecture, for vibration isolation

Figure 2.3: Example of Stewart platforms. (a) [29] and (b) [30]

MIMO robust control strategies

The NASS inherently involves multi-input, multi-output (MIMO) feedback control. The control system must process position measurements from the online metrology system and reference positions derived from the desired micro-station movements, commanding the active platform in real time to stabilize the sample and compensate for all error sources, including stage imperfections, thermal drifts, and vibrations. Ensuring the stability and robustness of these feedback loops is paramount, especially within the demanding operational context of a synchrotron beamline, which requires reliable 24/7 operation with minimal intervention. This contrasts with many traditional synchrotron instruments built using proven, passively stable components like stepper motors and conventional bearings.

Several factors complicate the design of robust feedback control for the NASS. The system must perform reliably across diverse experimental conditions, including different scan types (tomography, linear scans) and velocities (slow drifts to fast fly-scans). The continuous rotation of the spindle introduces gyroscopic coupling effects and means actuators rotate relative to stationary sensors, altering the system dynamics. Perhaps the most significant challenge is the wide variation in payload mass, from potentially 1 kg up to 50 kg. High-performance positioning controllers often assume a fixed, well-characterized payload,

as seen in applications like lithography or atomic force microscopy (AFM). Designing for robustness against large payload variations typically necessitates larger stability margins, which can compromise achievable performance. Furthermore, unlike many systems where the active stage and sample are significantly lighter than the underlying coarse stages, the NASS payload mass can be substantially greater than the mass of the micro-station's top stages. This leads to strong dynamic coupling between the active platform and the micro-station structure, resulting in a more complex MIMO system with significant cross-talk between axes. These variations in operating conditions and payload translate into significant uncertainty or changes in the plant dynamics that the controller must handle. Therefore, the feedback controller must be designed to be robust against this plant uncertainty while still delivering the required nanometer-level performance.

Predictive Design / Mechatronics approach

The overall performance of the NASS will be determined by the interplay of numerous factors, including sensor accuracy and noise, actuator force and bandwidth, mechanical design stiffness and resonances, and the achievable control bandwidth. To navigate this complexity and ensure the final system meets its stringent specifications, a predictive design methodology, specifically a mechatronics approach, is essential. The goal is to rigorously evaluate different concepts, predict performance limitations, and guide the design process towards an optimal solution that functions correctly upon first assembly, given the significant cost and complexity involved. Key challenges within this approach include developing appropriate design methodologies, creating accurate simulation models capable of comparing different concepts quantitatively, and converging on a final design that demonstrably achieves the target performance levels.

3 Original Contributions

This thesis presents several original contributions aimed at addressing the challenges inherent in the design, control, and implementation of the Nano Active Stabilization System, primarily within the fields of Control Theory, Mechatronics Design, and Experimental Validation.

6DoF vibration control of a rotating platform

While long stroke-short stroke architectures have been implemented for 1-DoF or 2-DoF systems, this work extends the concept to a fully coupled 6-DoF system operating on a continuously rotating base. The active platform is designed not merely to correct rotational errors but to simultaneously compensate for errors originating from all underlying micro-station stages. The application of a continuously rotating Stewart platform for active vibration control and error compensation in this manner is believed to be novel in the reviewed literature.

Mechatronics design approach

A rigorous mechatronics design methodology was applied consistently throughout the NASS development lifecycle [31], [32]. Although the mechatronics approach itself is not new, its comprehensive application here, from initial concept evaluation using simplified models to detailed design optimization and experimental validation informed by increasingly sophisticated models, is noteworthy. Dynamical models were employed at every stage: for initial concept selection, detailed component optimization, understanding experimental observations, and optimizing control strategies. This thesis documents this process chronologically, illustrating how models of varying complexity can be effectively utilized at different project phases and how design decisions were systematically based on quantitative model predictions and analyses. While the resulting system is highly specific, the documented effectiveness of this integrated design approach may contribute to the broader adoption of mechatronics methodologies in the design of future synchrotron instrumentation.

Multi-body simulations with reduced order flexible bodies obtained by FEA

A key enabling tool employed extensively in this work was a combined multi-body simulation and Finite Element Analysis technique, specifically utilizing Component Mode Synthesis (CMS) to represent flexible bodies within the multi-body framework [33]. This hybrid approach, while established, was experimentally validated in this work for components critical to the NASS, namely amplified piezoelectric actuators and flexible joints. It proved invaluable for designing and optimizing components intended for integration into a larger, complex dynamic system. This methodology, detailed in Section [...], is presented as a potentially useful tool for future mechatronic instrument development.

Control Robustness by design

Addressing the critical challenge of robustness across varying experimental conditions (rotation speeds, payloads up to 50 kg) was approached through "robustness by design" rather than relying solely on complex robust control synthesis techniques (like $\mathcal{H}_\infty$ or μ-synthesis). The strategy involved selecting a system architecture (mechanics, sensors, actuators) inherently conducive to robust control. An example is the deliberate use of collocated actuator/sensor pairs, enabling the potential application of passivity-based control principles to guarantee stability. Informed architectural choices were made by systematically evaluating different sensor combination strategies (e.g., HAC/LAC, sensor fusion, two-sensor control) and comparing various MIMO decoupling approaches. This comparative analysis of control architectures, presented in Section [...], was identified as somewhat lacking in existing literature.

Active Damping of rotating mechanical systems using Integral Force Feedback

During conceptual design, it was found that the guaranteed stability properties of the established active damping technique known as Integral Force Feedback (IFF) are compromised when applied to rotating platforms like the NASS. To address this instability issue, two modifications to the classical IFF control scheme were proposed and analyzed. The first involves a minor adjustment to the control law itself, while the second incorporates physical springs in parallel with the force sensors. Stability conditions and optimal parameter tuning guidelines were derived for both modified schemes. This is further discussed in Section [...] and was the subject of publications [34], [35].

Design of complementary filters using $\mathcal{H}_\infty$ Synthesis

For implementing sensor fusion, where signals from multiple sensors are combined, complementary filters are often employed. A novel method for designing these filters using $\mathcal{H}_\infty$ synthesis techniques was developed [36]. This method allows explicit shaping of the filter norms, providing guarantees on the performance of the sensor fusion process. This design strategy, discussed further in Section [...], has subsequently found application in optimizing sensor fusion for gravitational wave detectors [37]. The integration of such filters into feedback control architectures can also lead to advantageous control structures, as proposed in [38] and further studied in Section [...].

Experimental validation of the Nano Active Stabilization System

The conclusion of this work involved the experimental implementation and validation of the complete NASS on the ID31 beamline. Experimental results demonstrate that the system successfully improves the effective positioning accuracy of the micro-station from its native ~10 µm level down to the target ~100 nm range during representative scientific experiments. Crucially, robustness to variations in sample mass (up to 39 kg tested) and diverse experimental conditions (e.g., tomography scans) was verified. The NASS thus provides a versatile end-station solution, uniquely combining high payload capacity with nanometer-level accuracy and stability, enabling optimal utilization of the advanced capabilities of the ESRF-EBS beam and associated detectors. To the author's knowledge, this represents the first demonstration of such a 5-DoF active stabilization platform being used to enhance the accuracy of a complex positioning system to this level.

4 Thesis Outline - Mechatronics Design Approach

This thesis is structured chronologically, mirroring the phases of the mechatronics development approach employed for the NASS project. It is divided into three chapters, each corresponding to a distinct phase of this methodology: Conceptual Design, Detailed Design, and Experimental Validation. A brief overview of each chapter's content, is provided below.

Conceptual design development

- Talk about dynamic error budgeting
- Talk about used model

The goal of this first chapter is to find a concept:

- that will provide the wanted performances with high level of confidence
- As such system is costly, a mechatronics design approach is used [39] to be able to design the system "right the first time":
  - When the system is finally build, its performance level should satisfy the specifications.
  - No significant changes are allowed in the post design phase.
  - Because of this, the designer wants to be able to predict the performance of the system a-priori and gain insight in the performance limiting factors of the system.

To do so:

- Dynamical models are used, with included disturbances, feedback architecture, etc.. These models can be used to perform simulations, evaluate performances
- General idea is to start with very simple models, that can easily be understood (mass-spring-damper uniaxial model)
- Increase the model complexity if important physical phenomenon are to be modelled (cf the rotating model)
- Only when better understanding of the physical effects in play, and only if required, go for higher model complexity (here multi-body model)

To better understand the performance limitations, for different models, *dynamic error budgeting* [39], [40] are performed. It consists of:

- Disturbance and noise signals are modeled by their spectral content, i.e. by their power spectral density (PSD)
- The effect of each error sources on the final error, while the feedback control is active, can be easily estimated
- Therefore, the effect that have the greatest impact on the achievable performance can be easily spotted and improved
- Different concepts can be compared
- This tool is therefore key in better understanding the main limitations, and guide the determination of the best concept, early in the project.

This chapter concludes with accurate time domain simulations of a tomography experiment, validating the developed concept.

Detailed design

- In the second chapter, the chosen concept can be design in more details.
- First, the architecture and geometry of the active platform is optimized.
- Then, key components of the active platform, such as the flexible joints and the actuators, are optimized using the combined multi-body / FEA design approach.
- This allowed to optimize the components using very accurate models (thanks to FEA), while still being able to integrate these components in the complete multi-body model of the NASS for time domain simulations.
- Different aspects of the control of the NASS, such as the optimal use of multiple sensors integrated in the active platform, the best adapted decoupling strategy and the design of the robust controller, are then discussed.
- The requirements for all the associated instrumentation (digital to analog converters, analog to digital converters, voltage amplifiers, relative motion sensors) are chosen based on dynamic error budgeting. Using such approach, it was made sure that none of these instrumentation will limit the overall performance of the system.
- This chapter concludes with a presentation of the final design of the active platform.

Experimental validation

After converging to a detailed design that give acceptable performance based on the models, the different parts were ordered and the experimental phase began.

Instead of directly assembling the active platform and testing it on the ID31 micro-station, a systematic approach was followed to characterize individual components.

- Therefore, actuators and flexible joints were individual characterized. This allowed to update the model of these components, and obtained a more accurate model of the active platform Systematic validation/refinement of models with experimental measurements

- Actuators and flexible joints were combined to form the active "struts" of the active platform. These struts are also characterized

- Once the active platform were assembled, its dynamical model were found to over a very good match with the measured dynamics.

- This chapter conclude with the experimental tests on the ID31 micro-station of the complete NASS.

- Various scientific experiments are performed, such as tomography, and with various payload masses, to access the performances of the final system.

Bibliography

[1] P. Raimondi, N. Carmignani, L. R. Carver, et al., "Commissioning of the hybrid multibend achromat lattice at the european synchrotron radiation facility," *Physical Review Accelerators and Beams*, vol. 24, no. 11, p. 110 701, 2021 (cit. on p. 4).

[2] V. Schoeppler, E. Reich, J. Vacelet, et al., "Shaping highly regular glass architectures: A lesson from nature," *Science Advances*, vol. 3, no. 10, eaao2047, 2017 (cit. on pp. 6, 7).

[3] C. Sanchez-Cano, I. Romero-Canelón, Y. Yang, et al., "Synchrotron x-ray fluorescence nanoprobe reveals target sites for organo-osmium complex in human ovarian cancer cells," *Chemistry - A European Journal*, vol. 23, no. 11, pp. 2512–2516, 2017 (cit. on pp. 6, 7).

[4] C. Riekel, "Microfocus workshop at the esrf," *Synchrotron Radiation News*, vol. 2, no. 1, pp. 8–9, 1989 (cit. on p. 8).

[5] R. Barrett, R. Baker, P. Cloetens, et al., "Reflective optics for hard x-ray nanofocusing applications at the esrf," *Synchrotron Radiation News*, vol. 29, no. 4, pp. 10–15, 2016 (cit. on p. 8).

[6] R. Barrett, *X-ray optics at accelerator-based light sources*, Presentation, 2024 (cit. on p. 8).

[7] W. Xu, H. Xu, D. Gavrilov, et al., "High-speed fly-scan capabilities for x-ray microscopy systems at nsls-ii," in *X-Ray Nanoimaging: Instruments and Methods VI*, Oct. 2023, nil (cit. on pp. 9, 12, 13).

[8] X. Huang, K. Lauer, J. N. Clark, et al., "Fly-scan ptychography," *Scientific Reports*, vol. 5, no. 1, p. 9074, 2015 (cit. on p. 9).

[9] T. Hatsui and H. Graafsma, "X-ray imaging detectors for synchrotron and xfel sources," *IUCrJ*, vol. 2, no. 3, pp. 371–383, 2015 (cit. on p. 9).

[10] C. Riekel, M. Burghammer, and R. Davies, "Progress in micro- and nano-diffraction at the esrf id13 beamline," *IOP Conference Series: Materials Science and Engineering*, vol. 14, no. nil, p. 012 013, 2010 (cit. on p. 10).

[11] S. J. Leake, G. A. Chahine, H. Djazouli, et al., "The nanodiffraction beamline id01/esrf: A microscope for imaging strain and structure," *Journal of Synchrotron Radiation*, vol. 26, no. 2, pp. 571–584, 2019 (cit. on p. 10).

[12] G. Martínez-Criado, J. Villanova, R. Tucoulou, et al., "Id16b: A hard x-ray nanoprobe beamline at the esrf for nano-analysis," *Journal of Synchrotron Radiation*, vol. 23, no. 1, pp. 344–352, 2016 (cit. on p. 11).

[13] J. Wright, C. Giacobbe, and M. Majkut, "New opportunities at the materials science beamline at esrf to exploit high energy nano-focus x-ray beams," *Current Opinion in Solid State and Materials Science*, vol. 24, no. 2, p. 100 818, 2020 (cit. on p. 11).

[14] C. G. Schroer, M. Seyrich, M. Kahnt, et al., "Ptynami: Ptychographic nano-analytical microscope at petra iii: Interferometrically tracking positions for 3d x-ray scanning microscopy using a ball-lens retroreflector," in *X-Ray Nanoimaging: Instruments and Methods III*, Sep. 2017 (cit. on pp. 11–13).

[15] F. Villar, L. Andre, R. Baker, et al., "Nanopositioning for the esrf id16a nano-imaging beamline," *Synchrotron Radiation News*, vol. 31, no. 5, pp. 9–14, 2018 (cit. on pp. 11–13).

[16] A. Schropp, R. Döhrmann, S. Botta, et al., "Ptynami: Ptychographic nano-analytical microscope," *Journal of Applied Crystallography*, vol. 53, no. 4, pp. 957–971, 2020 (cit. on pp. 11–13).

[17] E. Nazaretski, K. Lauer, H. Yan, et al., "Pushing the limits: An instrument for hard x-ray imaging below 20 nm," *Journal of Synchrotron Radiation*, vol. 22, no. 2, pp. 336–341, 2015 (cit. on pp. 12, 13).

[18] T. Stankevic, C. Engblom, F. Langlois, et al., "Interferometric characterization of rotation stages for x-ray nanotomography," *Review of Scientific Instruments*, vol. 88, no. 5, p. 053 703, 2017 (cit. on pp. 12, 13).

[19] C. Engblom et al., "Nanoprobe results: Metrology & control in stacked closed-loop systems," in *Proc. of International Conference on Accelerator and Large Experimental Control Systems (ICALEPCS'17)*, JACoW, Jan. 2018 (cit. on pp. 12, 13).

[20] E. Nazaretski, D. S. Coburn, W. Xu, et al., "A new kirkpatrick-baez-based scanning microscope for the submicron resolution x-ray spectroscopy (srx) beamline at nsls-ii," *Journal of Synchrotron Radiation*, vol. 29, no. 5, pp. 1284–1291, 2022 (cit. on pp. 12–14).

[21] M. Holler, J. Raabe, R. Wepf, et al., "Omny pin-a versatile sample holder for tomographic measurements at room and cryogenic temperatures," *Review of Scientific Instruments*, vol. 88, no. 11, p. 113 701, 2017 (cit. on pp. 12, 13).

[22] M. Holler, J. Raabe, A. Diaz, et al., "Omny-a tomography nano cryo stage," *Review of Scientific Instruments*, vol. 89, no. 4, p. 043 706, 2018 (cit. on pp. 12, 13).

[23] J. Kelly, A. Male, N. Rubies, et al., "The delta robot-a long travel nano-positioning stage for scanning x-ray microscopy," *Review of Scientific Instruments*, vol. 93, no. 4, nil, 2022 (cit. on pp. 12–14).

[24] R. R. Geraldes, G. B. Z. L. Moreno, F. R. Lena, et al., "The high-dynamic cryogenic sample stage for sapoti/carnaúba at sirius/lnls," in *Proceedings of XRM2022*, Jan. 2023, nil (cit. on pp. 12, 13).

[25] J. Wang, Y.-c. K. Chen, Q. Yuan, et al., "Automated markerless full field hard x-ray microscopic tomography at sub-50 nm 3-dimension spatial resolution," *Applied Physics Letters*, vol. 100, no. 14, p. 143 107, 2012 (cit. on pp. 12, 13).

[26] E. Nazaretski, H. Yan, K. Lauer, et al., "Design and performance of an x-ray scanning microscope at the hard x-ray nanoprobe beamline of nsls-ii," *Journal of Synchrotron Radiation*, vol. 24, no. 6, pp. 1113–1119, 2017 (cit. on p. 13).

[27] H. Shinno, H. Yoshioka, and H. Sawano, "A newly developed long range positioning table system with a sub-nanometer resolution," *CIRP Annals*, vol. 60, no. 1, pp. 403–406, 2011 (cit. on p. 15).

[28] R. M. Schmidt, G. Schitter, and A. Rankers, *The Design of High Performance Mechatronics - Third Revised Edition*. Ios Press, 2020 (cit. on p. 15).

[29] Z. Du, R. Shi, and W. Dong, "A piezo-actuated high-precision flexible parallel pointing mechanism: Conceptual design, development, and experiments," *IEEE Transactions on Robotics*, vol. 30, no. 1, pp. 131–137, 2014 (cit. on p. 19).

[30] G. Hauge and M. Campbell, "Sensors and control of a space-based six-axis vibration isolation system," *Journal of Sound and Vibration*, vol. 269, no. 3-5, pp. 913–931, 2004 (cit. on p. 19).

[31] T. Dehaeze, M. Magnin Mattenet, and C. Collette, "Sample stabilization for tomography experiments in presence of large plant uncertainty," in *MEDSI'18*, (Paris, France), ser. Mechanical Engineering Design of Synchrotron Radiation Equipment and Instrumentation, Geneva, Switzerland: JACoW Publishing, Dec. 2018, pp. 153–157 (cit. on p. 21).

[32] T. Dehaeze, J. Bonnefoy, and C. Collette, "Mechatronics approach for the development of a nano-active-stabilization-system," in *MEDSI'20*, (Chicago, USA), ser. Mechanical Engineering Design of Synchrotron Radiation Equipment and Instrumentation, JACoW Publishing, 2021 (cit. on p. 21).

[33] P. Brumund and T. Dehaeze, "Multibody simulations with reduced order flexible bodies obtained by fea," in *MEDSI'20*, (Chicago, USA), ser. Mechanical Engineering Design of Synchrotron Radiation Equipment and Instrumentation, JACoW Publishing, 2021 (cit. on p. 22).

[34] T. Dehaeze and C. Collette, "Active damping of rotating platforms using integral force feedback," in *Proceedings of the International Conference on Modal Analysis Noise and Vibration Engineering (ISMA)*, 2020 (cit. on p. 23).

[35] T. Dehaeze and C. Collette, "Active damping of rotating platforms using integral force feedback," *Engineering Research Express*, Feb. 2021 (cit. on p. 23).

[36] T. Dehaeze, M. Vermat, and C. Collette, "Complementary filters shaping using $\mathcal{H}_\infty$ synthesis," in *7th International Conference on Control, Mechatronics and Automation (ICCMA)*, 2019, pp. 459–464 (cit. on p. 23).

[37] T. T. L. Tsang, T. G. F. Li, T. Dehaeze, and C. Collette, "Optimal sensor fusion method for active vibration isolation systems in ground-based gravitational-wave detectors," *Classical and Quantum Gravity*, vol. 39, no. 18, p. 185 007, 2022 (cit. on p. 23).

[38] M. Verma, T. Dehaeze, G. Zhao, J. Watchi, and C. Collette, "Virtual sensor fusion for high precision control," *Mechanical Systems and Signal Processing*, vol. 150, p. 107 241, 2020 (cit. on p. 23).

[39] W. Monkhorst, "Dynamic error budgeting, a design approach," Ph.D. dissertation, Delft University, 2004 (cit. on pp. 24, 25).

[40] A. Okyay, "Mechatronic design, dynamics, controls, and metrology of a long-stroke linear nanopositioner," Ph.D. dissertation, University of Waterloo, 2016 (cit. on p. 25).